7. L. Addadi, S. Raz, S. Weiner, *Adv. Mater. (Deerfield Beach Fla.)* **15**, 959 (2003).
8. Y. Politi, T. Arad, E. Klein, S. Weiner, L. Addadi, *Science* **306**, 1161 (2004).
9. E. D. Eanes, I. H. Gillessen, A. S. Posner, *Nature* **208**, 365 (1965).
10. V. Pipich, M. Balz, S. E. Wolf, W. Tremel, D. Schwahn, *J. Am. Chem. Soc.* **130**, 6879 (2008).
11. A. Berman *et al.*, *Science* **250**, 664 (1990).
12. J. Aizenberg *et al.*, *FASEB J.* **9**, 262 (1995).
13. J. Aizenberg *et al.*, *Chemistry* **1**, 414 (1995).
14. F. C. Meldrum, H. Cölfen, *Chem. Rev.* **108**, 4332 (2008).
15. M. M. Murr, D. E. Morse, *Proc. Natl. Acad. Sci. U.S.A.* **102**, 11657 (2005).
16. H. C. Schröder, X. Wang, W. Tremel, H. Ushijima, W. E. G. Müller, *Nat. Prod. Rep.* **25**, 455 (2008).
17. J. Küther, R. Seshadri, W. Knoll, W. Tremel, *J. Mater. Chem.* **8**, 641 (1998).
18. P. R. Carey, *Biochemical Applications of Raman and Resonance Raman Spectroscopies* (Academic Press, New York, 1982), chap. 4.
19. W. E. G. Müller *et al.*, *Cell Tissue Res.* **321**, 285 (2005).
20. H. Cölfen, M. Antonietti, *Mesocrystals and Nonclassical Crystallization* (Wiley, Chichester, 2008).
21. Y. Politi *et al.*, *Proc. Natl. Acad. Sci. U.S.A.* **105**, 17362 (2008).
22. C. Levi, J. L. Barton, C. Guillemet, E. Lebras, P. A. Lehuede, *J. Mater. Sci. Lett.* **8**, 337 (1989).
23. M. Sarikaya *et al.*, *J. Mater. Res.* **16**, 1420 (2001).
24. A. Woesz *et al.*, *J. Mater. Res.* **21**, 2068 (2006).
25. M. Johnson, S. L. Walter, B. D. Flinn, G. Mayer, *Acta Biomater.* **6**, 2181 (2010).
26. A. Miserez *et al.*, *Adv. Funct. Mater.* **18**, 1241 (2008).
27. R. B. Emlett, *Biol. Bull.* **163**, 264 (1982).
28. P. L. O'Neill, *Science* **213**, 646 (1981).
29. P. U. P. A. Gilbert, F. H. Wilt, in *Molecular Biomineralization*, W. E. G. Müller, Ed. (Springer-Verlag, Heidelberg, 2011), pp. 199–223.

Acknowledgments: This work was partially supported by the Deutsche Forschungsgemeinschaft within the SPP 1420. T.P.C. was supported by a Deutscher Akademischer Austauschdienst scholarship. We acknowledge the use of the facilities of the EM Center in Mainz (EZMZ) supported by the Center for Complex Matter and the SFB 625. We are grateful to R. Jung-Pothmann for performing single-crystal x-ray measurements and J. Ally for insightful discussions. The authors declare that they have no competing financial interests.

Supplementary Materials

www.sciencemag.org/cgi/content/full/339/6125/1298/DC1
Materials and Methods
Figs. S1 to S18
References
Movies S1 to S3

7 November 2011; accepted 24 January 2013
10.1126/science.1216260

Real-Time Observation of Surface Bond Breaking with an X-ray Laser

M. Dell'Angela,[1] T. Anniyev,[2] M. Beye,[2,3] R. Coffee,[4] A. Föhlisch,[3,5] J. Gladh,[6] T. Katayama,[2] S. Kaya,[2] O. Krupin,[4,7] J. LaRue,[2] A. Møgelhøj,[8,9] D. Nordlund,[10] J. K. Nørskov,[8,11] H. Öberg,[6] H. Ogasawara,[10] H. Öström,[6] L. G. M. Pettersson,[6] W. F. Schlotter,[4] J. A. Sellberg,[2,6] F. Sorgenfrei,[1] J. J. Turner,[4] M. Wolf,[12] W. Wurth,[1] A. Nilsson[2,6,8,10]*

We used the Linac Coherent Light Source free-electron x-ray laser to probe the electronic structure of CO molecules as their chemisorption state on Ru(0001) changes upon exciting the substrate by using a femtosecond optical laser pulse. We observed electronic structure changes that are consistent with a weakening of the CO interaction with the substrate but without notable desorption. A large fraction of the molecules (30%) was trapped in a transient precursor state that would precede desorption. We calculated the free energy of the molecule as a function of the desorption reaction coordinate using density functional theory, including van der Waals interactions. Two distinct adsorption wells—chemisorbed and precursor state separated by an entropy barrier—explain the anomalously high prefactors often observed in desorption of molecules from metals.

The most fundamental elementary surface chemical process, the adsorption of a molecule, has been proposed to proceed through a weakly bound "precursor" state (*1*–*4*) that helps the molecule lose rotational and translation energy before forming a chemisorption bond to the surface. This transient state has never been directly detected in terms of a spectroscopic signature, although ultrafast vibrational spectroscopy measurements with pump-probe techniques have the potential to detect short-lived transient species on surfaces (*5*–*10*). A transient shift of the vibrational frequency of thermally highly excited adsorbed CO molecules has been detected by using pump-probe sum frequency generation (SFG) spectroscopy. However, the shifts were mostly attributed to excitation of frustrated rotational motions that led to diffusive motion parallel to the surface (hopping between adsorption sites), rather than to a weakly adsorbed precursor state (*7*–*9*, *11*).

We show that ultrafast pump-probe x-ray fluorescence spectroscopic techniques based on an x-ray free-electron laser, the Linac Coherent Light Source (LCLS), can be used to probe the electronic structure of a transiently populated, weakly adsorbed state in CO desorption from Ru(0001). An optical laser pump pulse increased the phonon temperature of the substrate on a sub-picosecond time scale (*12*) and rapidly populated the adsorbate transient state as an intermediate prior to desorption. The time evolution of the occupied and unoccupied valence electronic structure around the adsorbed CO molecule on Ru(0001) could be followed in an element-specific way during the desorption process with the use of oxygen-resonant x-ray emission spectroscopy (XES) and x-ray absorption spectroscopy (XAS), respectively. In particular, the CO molecules in the transient state had an electronic structure closer to the gas phase than to the chemisorbed state; however, the antibonding CO $2\pi^*$ states were still substantially affected by the interaction with the surface. Combining the experimental data with results of free energy calculations based on density functional theory (DFT) by using a new functional that includes van der Waals interactions identified a precursor state, a two-dimensional gas of CO molecules that weakly interacts with the surface but still affects desorption kinetics.

The principle of core-level excitation (XAS) and de-excitation (XES) (*13*) is illustrated in Fig. 1, middle, together with the static spectra from the oxygen atom for CO chemisorbed on Ru(0001). Core-level spectroscopies constitute element-specific probes of the electronic structure, both the occupied (XES) and unoccupied (XAS) states, through the involvement of the local O 1*s* level (*14*, *15*). Investigations of the chemical bonding of CO to late-transition metal and noble-metal surfaces by means of XES in combination with DFT calculations (*14*, *16*) show that the key interaction is that of the 1π- and $2\pi^*$-orbitals of the molecule with the metal *d*-states, resulting in an allylic configuration, as well as the polarization of the 5σ-orbital from the C to the O atom and a shift to higher-binding energy than gas phase. The lowest in energy of the three orbitals resulting from the π-interaction is the $1\tilde{\pi}$ orbital in a bonding configuration with the metal; the tilde denotes that the orbital has mixed with surface-metal orbitals. The middle orbital (denoted $\tilde{d}_\pi$) is nonbonding and mainly of *d*-character with a lone-pair contribution on the O atom, whereas the highest

[1]University of Hamburg and Center for Free Electron Laser Science, Luruper Chausse 149, D-22761 Hamburg, Germany. [2]Stanford Institute for Materials Energy Sciences (SIMES), SLAC National Accelerator Laboratory, 2575 Sand Hill Road, Menlo Park, CA 94025, USA. [3]Institute for Methods and Instrumentation in Synchrotron Radiation Research, Helmholtz-Zentrum Berlin für Materialien und Energie GmbH, Wilhelm-Conrad-Röntgen Campus, Albert-Einstein-Strasse 15, 12489 Berlin, Germany. [4]Linac Coherent Light Source, SLAC National Accelerator Laboratory, 2575 Sand Hill Road, Menlo Park, CA 94025, USA. [5]Institut für Physik und Astronomie, Universität Potsdam, Karl-Liebknecht-Strasse 24-25, 14476 Potsdam, Germany. [6]Department of Physics, AlbaNova University Center, Stockholm University, SE-10691, Sweden. [7]European X-Ray Free Electron Laser (XFEL) GmbH, Albert-Einstein-Ring 19, 22761 Hamburg, Germany. [8]Sustainable Energy Through Catalysis (SUNCAT) Center for Interface Science and Catalysis, SLAC National Accelerator Laboratory, 2575 Sand Hill Road, Menlo Park, CA 94025, USA. [9]Center for Atomic-Scale Materials Design (CAMD), Department of Physics, Technical University of Denmark, DK 2800 Lyngby, Denmark. [10]Stanford Synchrotron Radiation Lightsource, SLAC National Accelerator Laboratory, 2575 Sand Hill Road, Menlo Park, CA 94025, USA. [11]SUNCAT Center for Interface Science and Catalysis, Department of Chemical Engineering, Stanford University, Stanford, CA 95305, USA. [12]Fritz-Haber Institute, Max Planck Society, Faradayweg 4-6, D-14195 Berlin, Germany.

*To whom correspondence should be addressed. E-mail: nilsson@slac.stanford.edu

orbital is the $2\tilde{\pi}^*$ level in an antibonding configuration lying mainly above the Fermi level E_F. The $2\tilde{\pi}^*$ level shifts toward E_F through mixing with the 1π orbital (*17*).

Dynamic information on the electronic structure obtained through resonant O $1s \rightarrow 2\tilde{\pi}^*$ excitation with a 100-fs pulse from the LCLS x-ray free-electron laser before and 12 ps after inducing a surface-temperature jump with a 400-nm optical laser pulse of 50 fs duration (*12*) is shown in Fig. 1. In the XES spectra, there were four major changes after excitation: (i) The peak containing the $5\tilde{\sigma}$ and $1\tilde{\pi}$ orbitals became sharper with a decrease in intensity of the shoulder at 523.5 eV and a shift to higher emission energy; (ii) the dip between the $4\tilde{\sigma}$ and $5\tilde{\sigma}$ spectral features was better resolved; (iii) the broad shoulder around 527 eV, where the $\tilde{d}_\pi$ was observed, decreased in intensity; and (iv) a peak centered around 533 eV appeared. This peak corresponds to participator decay, in which the excited electron remains on the CO molecule and returns to the core level with emission of an x-ray photon of similar energy as the excitation (*12*). In the XAS spectra, we observed both a shift toward higher absorption energies and higher intensities of the $2\tilde{\pi}^*$ resonance. All of the observed spectral changes in the electronic structure are consistent with a substantial fraction of CO molecules being more weakly bound to the surface.

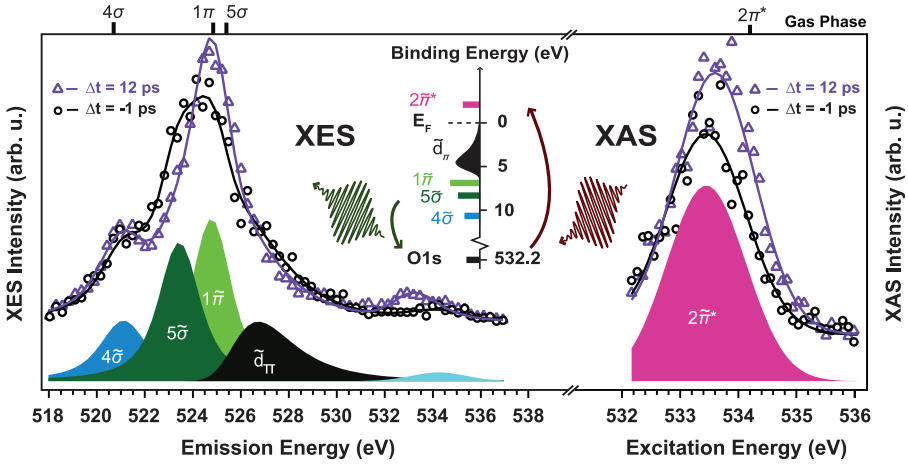

Fig. 1. Oxygen K-edge XES (left) and XAS (right) spectra (markers) of CO/Ru(0001) and corresponding fits (solid lines) measured at two selected pump-probe delays. At the bottom of the two panels, the peak deconvolution resulting from the fit of the spectra acquired at $\Delta t = -1$ ps is shown. The XAS data have been fitted with a Gaussian peak for the O1*s* $\rightarrow 2\tilde{\pi}^*$ resonance. The XES spectra have been fitted with three peaks of Voigt lineshape for the $1\tilde{\pi}$, $5\tilde{\sigma}$, and $4\tilde{\sigma}$ orbitals and an asymmetric Gaussian for the $\tilde{d}_\pi$ states; the elastic peak is indicated in light blue around 534 eV. The fit of the spectra at $\Delta t = 12$ ps has been performed by varying only intensity and position of the previously determined components. (**Top**) The positions of the fitted components measured in previous resonant gas phase experiments are also indicated (*26*). (**Middle**) A schematic illustration of the excitation process from the O1*s* level to the unoccupied $2\tilde{\pi}^*$ resonance in XAS and the core hole decay process from occupied molecular orbitals back to the O1*s* in XES.

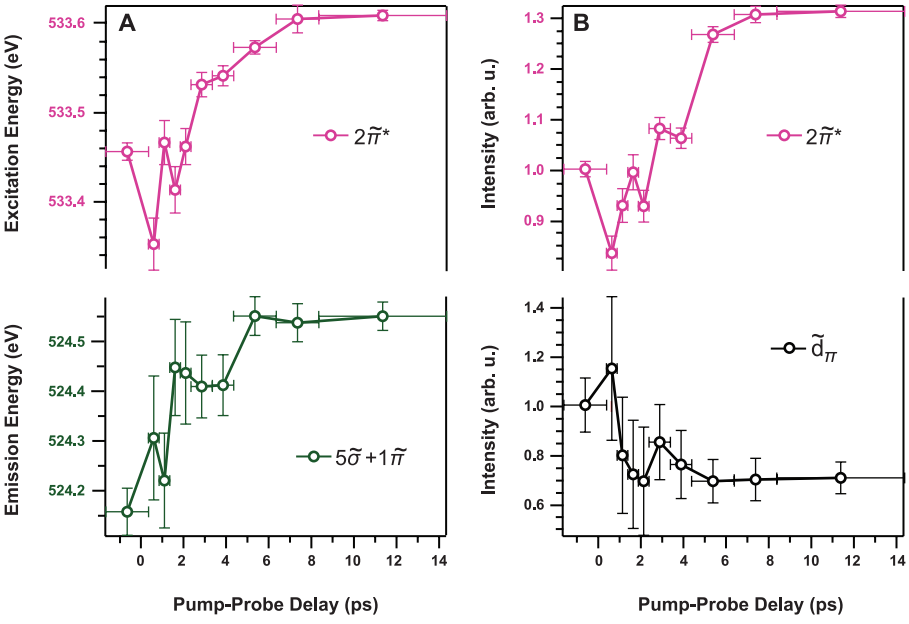

Fig. 2. (**A** and **B**) Experimental observations indicating the population of a weakly adsorbed precursor state before the desorption of CO from Ru(0001). The intensities in (B) have been normalized to the unpumped data ($\Delta t = -1$ps). Because the pump-probe delay was continuously scanned during the measurement, the error bars in the plots along the time axis indicate the length of the time interval in which the data have been summed to produce the spectra of Fig. 1. The error bars on the other axis are evaluated from the fits (1σ), where each point in the measured spectrum has been statistically weighted.

We refined these spectral observations using peak fitting (*12*) and show the evolution of the peaks with pump-probe delay time in Fig. 2. In Fig. 2A, we display only the average of the $5\tilde{\sigma}$ and $1\tilde{\pi}$ peak positions in order to have a parameter that is independent of the details of the fitting procedure. All of the changes reached a maximum after 6 to 10 ps, after which they were nearly constant. The main peak in the XES spectra—the center of mass of the $1\tilde{\pi}$ and $5\tilde{\sigma}$ components—moves toward higher emission energy, toward that for gas-phase CO, which is consistent with a weakening of the bond between CO and metal. The overall shift of the combined $5\tilde{\sigma}$ and $1\tilde{\pi}$ peak mostly originates from changes in the $5\tilde{\sigma}$ position. Bond weakening is also consistent with the decrease in the intensity of the $\tilde{d}_\pi$ spectral feature, in which only 70% of the intensity remains after long delay times (Fig. 2B). The $2\tilde{\pi}^*$ level (Fig. 2A) shifts toward the $2\pi^*$ value at 534.2 eV; the intensity at the gas-phase energy position is still low, indicating that few molecules have completely desorbed. The bonding to the surface leads to partial occupation of CO $2\pi^*$ character in the $\tilde{d}_\pi$ orbital, resulting in a decrease of the $2\tilde{\pi}^*$ XAS resonance intensity (*16*, *17*). The gas-phase $2\pi^*$ resonance intensity is also partly restored with increasing delay time. The latter is directly related to the observed increase in the participator peak because we use O1*s* $\rightarrow 2\tilde{\pi}^*$ excitation, and for a weaker interaction with the surface, the excited electron is less likely to couple to the metal and delocalize.

Laser-induced surface reactions on metals are driven by hot electrons excited in the substrate, which couple to the adsorbate and substrate phonons within the first picosecond (*12*). We observed some changes at early times (at 1 ps, as seen in Fig. 2) that we attribute to hot electrons exciting frustrated rotations and translation of the CO molecules on the surface in accordance with previous studies (*7*, *8*, *18*). However, the hot electron bath transfers energy to phonons within 1 to 2 ps that

subsequently couple to the CO molecule. Because the major bond-weakening occurred only after a few picoseconds, we can directly relate this change to an increase in the surface temperature (*12*).

Our DFT calculations of the adsorption energy of CO using the Bayesian error estimation functional (*19*) includes the nonlocal correlation effects, giving rise to van der Waals interactions (*20*). When plotted at 0 K as a function of the distance of the CO molecule to the surface (Fig. 3), the chemisorbed state has an adsorption energy of 1.4 eV versus an experimental value of 1.6 eV (*21*). The dynamics at elevated temperatures was explored following Doren and Tully (*2*, *22*) by calculating $W(s)$, the potential of mean force (PMF), which is a free-energy curve including contributions from entropy as a function of the reaction coordinate s:

$$W(s) = -k_B T \ln[g(s)] + k_B T \ln[g(\infty)] \quad (1)$$

$$g(s) = \Gamma^{-1} \int e^{\frac{V(s,\boldsymbol{q})}{k_B T}} d\boldsymbol{q} \quad (2)$$

Here, k_B is Boltzmann's constant, T is the temperature, s is the distance from the surface to the center of mass of the CO molecule along the reaction coordinate, $\boldsymbol{q}$ represents all degrees of freedom except the reaction coordinate, $V(s,\boldsymbol{q})$ is the interaction potential, and Γ is an arbitrary normalization constant. All degrees of freedom except the reaction coordinate have been thermally averaged. Although Eq. 1 assumes that all degrees of freedom can be treated classically—which is a rather crude approximation, especially at low temperatures—it can provide qualitative insights; for example, Gibbs free energy ($\Delta G°$) of the extrema directly provides the transition-state theory rate constant for desorption (or adsorption).

As shown in Fig. 3, as the temperature increases two minima develop in the potential of mean force: the chemisorption minimum and another minimum at greater distances that we associated with a precursor state for adsorption or desorption (*2*, *22*). At high temperature, the loss of entropy in the strongly adsorbed state, in which the rotations and translations of the CO molecule are frustrated, means that the free energy increases substantially relative to the gas phase. In the precursor state, the CO molecule is nearly free to rotate and to move parallel to the surface to the extent allowed by the finite coverage. Here, the entropy loss is minimal.

The following qualitative explanation of the experimental results is suggested with Fig. 3. After the laser pulse, the adsorbate temperature increases to a value in the range of 1500 to 2000 K (*12*). Here, the free energy $W(s)$ of the precursor state becomes comparable with that of the chemisorbed state, and a substantial fraction of the adsorbed CO molecules shift to the precursor state. Do the observed changes in the XES and XAS spectra correspond to a population of CO molecules in the precursor state? The core hole state in XES is prepared by exciting an O1s electron to the 2π* level. For chemisorbed CO, this electron transfers to the substrate faster than the core hole decays and has no influence on the XES spectrum (*14*, *23*), but in the gas phase, it is localized on the molecule and screens the various final valence hole states, giving rise to a spectator shift (*24*); an additional peak, due to participator decay in which the excited electron decays back to the ground state, furthermore appears at an energy similar to the exciting photon (*24*). Shown in Fig. 4, left, is a fit of the 12-ps XES spectrum in terms of a linear combination consisting of 70% chemisorbed unpumped CO spectrum and 30% of an appropriately adjusted gas-phase CO spectrum (*12*). Compared with gas phase, the 4σ and 1π peaks need to be shifted by 0.3 and 0.1 eV, respectively, toward higher energies, which indicates that the spectator shift is smaller than in the gas phase; the larger shift of 4σ than 1π required for the fit of our data is consistent with the larger gas-phase spectator shift for 4σ (1.8 eV) than for 1π (0.8 eV). The participator decay of the excited electron is shifted by 0.5 eV toward lower energy and contributes with only half the intensity, showing that at long time delays, the excited 2π* electron is less localized on the CO molecule in comparison with when in the gas phase. The down energy shift in the participator decay is also consistent with the fit of the XAS spectrum at 12-ps delay (Fig. 4, right), which results in a similar ratio of unpumped chemisorbed CO with the resonance shifted by 0.3 eV relative to gas phase.

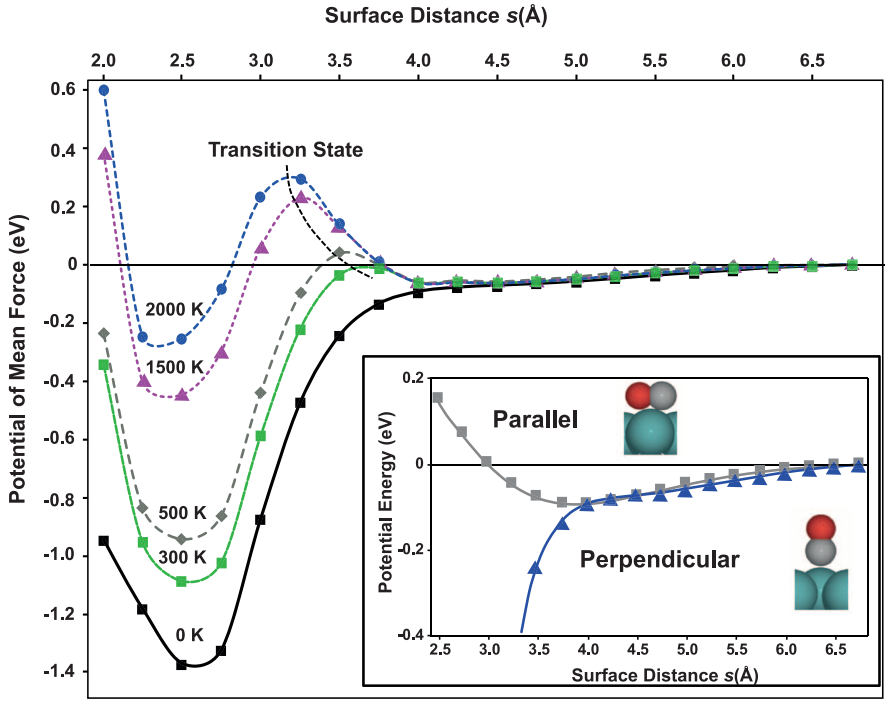

Fig. 3. The potential of mean force for CO adsorption/desorption on Ru(0001) at 0 K (minimum energy path) and 300, 500, 1500, and 2000 K. (**Inset**) The potential energy curve (0 K) of the CO molecule with orientation parallel and perpendicular to the Ru(0001) surface. The surface distance is measured between the CO center of mass and the surface. At 0 K and distances smaller than 2.5 Å, CO moves from on-top to bridge and hollow sites, giving less strong repulsion as compared with the finite temperatures at which more repulsive orientations are sampled.

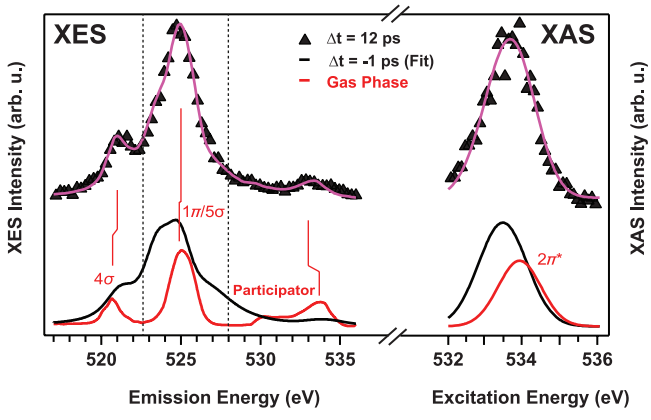

Fig. 4. (**Left**) XES and (**Right**) XAS at a pump-probe delay of 12 ps were represented by a sum of spectra corresponding to unpumped chemisorbed CO obtained from the spectra at negative delay and precursor state spectra represented by an appropriately adjusted gas-phase spectrum (*12*). The resulting fit (pink) and 12-ps experimental data are vertically offset for clarity.

The difference in XAS and participator decay positions of the 2π* state can be related to nuclear dynamics during the core hole lifetime in XES (*24*). The smaller spectator shift in XES, lower participator intensity of the excited 2π* electron, and less shifted 2π* XAS resonance show that the CO molecules that have broken the direct CO metal bond have not yet desorbed into gas phase but still interact weakly with the surface.

Using DFT, we examined (figs. S9 and S10) the 1s→2π* core-excited states and spectra for different points along the minimum energy path of Fig. 3. The computed XAS spectra reproduce the expected behavior with enhanced 2π* intensity together with a shift to higher energy as the distance to the surface increases. In the precursor state, the antibonding CO orbitals, which have a large spatial extent, still interact with the metal states. The substrate interaction with the 2π* has a distance dependence in the precursor state, and most likely, we are probing a distribution of distances in the experiment; rotation of the molecule in the precursor potential has only minor effects on the spectra (fig. S10).

Because 30% of the $\tilde{d}_\pi$ intensity disappeared and the spectra could be fitted with 30% shifted gas-phase contributions at long delay times, it is likely that 30% of the molecules were pumped into the precursor state, supporting the notion that the two states have rather comparable free energies. Some of the molecules desorb during the experiment, but when the system cools, the remaining molecules can return from the precursor to the chemisorbed state. Previous SFG results showed that the C-O stretch intensity was reduced by one order of magnitude after a pump laser pulse that led to a final desorption of ~30% of the adsorbed CO molecules (*8*, *12*). However, the SFG intensity recovered to half of its initial value after 170 ps (*8*) because roughly half of the molecules readsorbed into the chemisorbed state. We suggest that the initial drop of intensity in the SFG experiment corresponds to essentially all of the molecules being pumped into the precursor state, in which the SFG signal would disappear because of orientational disordering of the CO molecules (*25*, *26*). Because the laser fluence in the SFG experiment and in the present experiment are similar, we propose that also in the present case, ~50% of the molecules return to the chemisorbed state from the precursor state as the substrate cools down and the temperature-induced entropic barrier to the chemisorbed state vanishes. The molecules in the precursor state have very weak interactions perpendicular to the surface, which leads to a small probability of obtaining the perpendicular momentum needed for desorption. Considering, on the other hand, the time-reversed situation, a similar trapping in the precursor state due to the entropic barrier must also occur in chemisorption.

The prefactors in Arrhenius expressions for desorption rates of molecules such as CO are often anomalously large (*27*). For instance, the prefactor for CO desorption on Ru(0001) has been found to be of the order 10^{14} to 10^{19} s^{-1}, depending on coverage (*21*), versus typical values between 10^{12} and 10^{13} s^{-1}; this has generally been explained by the difference in entropy between the initial (adsorbed) state and the final (gas) state (*21*). We instead found that it is the entropy gain at the free-energy barrier between the chemisorbed and precursor state that is decisive. In the present case, this leads to a computed prefactor on the order of 10^{17} s^{-1} and, consequently, to the efficient population of the precursor state observed in our experiment.

References and Notes

1. A. Cassuto, D. A. King, *Surf. Sci.* **102**, 388 (1981).
2. D. J. Doren, J. C. Tully, *Langmuir* **4**, 256 (1988).
3. P. Kisliuk, *J. Phys. Chem. Solids* **3**, 95 (1957).
4. J. B. Taylor, I. Langmuir, *Phys. Rev.* **44**, 423 (1933).
5. C. Frischkorn, M. Wolf, *Chem. Rev.* **106**, 4207 (2006).
6. H. Arnolds, M. Bonn, *Surf. Sci. Rep.* **65**, 45 (2010).
7. E. H. G. Backus, A. Eichler, A. W. Kleyn, M. Bonn, *Science* **310**, 1790 (2005).
8. M. Bonn *et al.*, *Phys. Rev. Lett.* **84**, 4653 (2000).
9. F. Fournier, W. Zheng, S. Carrez, H. Dubost, B. Bourguignon, *J. Chem. Phys.* **121**, 4839 (2004).
10. I. M. Lane, D. A. King, Z. P. Liu, H. Arnolds, *Phys. Rev. Lett.* **97**, 186105 (2006).
11. K. Inoue, K. Watanabe, Y. Matsumoto, *J. Chem. Phys.* **137**, 024704 (2012).
12. Materials and methods, and supporting analysis of the experimental and theoretical data, are available as supplementary materials on *Science* Online
13. A. Föhlisch, W. Wurth, M. Stichler, C. Keller, A. Nilsson, *J. Chem. Phys.* **121**, 4848 (2004).
14. A. Nilsson, L. G. M. Pettersson, *Surf. Sci. Rep.* **55**, 49 (2004).
15. A. Nilsson *et al.*, *Phys. Rev. Lett.* **78**, 2847 (1997).
16. A. Föhlisch *et al.*, *J. Chem. Phys.* **112**, 1946 (2000).
17. O. Björneholm *et al.*, *Phys. Rev. B* **46**, 10353 (1992).
18. L. Bartels, F. Wang, D. Möller, E. Knoesel, T. F. Heinz, *Science* **305**, 648 (2004).
19. J. Wellendorff *et al.*, *Phys. Rev. B* **85**, 235149 (2012).
20. M. Dion, H. Rydberg, E. Schröder, D. C. Langreth, B. I. Lundqvist, *Phys. Rev. Lett.* **92**, 246401 (2004).
21. H. Pfnür, P. Feulner, D. Menzel, *J. Chem. Phys.* **79**, 4613 (1983).
22. D. J. Doren, J. C. Tully, *J. Chem. Phys.* **94**, 8428 (1991).
23. C. Keller *et al.*, *Phys. Rev. Lett.* **80**, 1774 (1998).
24. P. Skytt *et al.*, *Phys. Rev. A* **55**, 134 (1997).
25. Y. R. Shen, *Principles of Non-Linear Optics* (Wiley-Interscience, New York, 2003)
26. J. H. Hunt, P. Guyot-Sionnest, Y. R. Shen, *Chem. Phys. Lett.* **133**, 189 (1987).
27. I. Chorkendorf, H. Niemantsverdriet, *Concepts of Modern Catalysis and Kinetics* (Wiley-VCH, Weinheim, Germany, 2003).

Acknowledgments: This work is supported by the U.S. Department of Energy (DOE), Office of Basic Energy Sciences, Division of Materials Sciences and Engineering, under contract DE-AC02-76SF00515; the DOE, Basic Energy Science through the SUNCAT Center for Interface Science and Catalysis; the Swedish National Research Council; the Danish Center for Scientific Computing; the Volkswagen Stiftung; the Alexander von Humboldt Foundation; and the Lundbeck Foundation. The spectrum calculations were performed on resources provided by the Swedish National Infrastructure for Computing (SNIC) at the High Performance Computing Center North. Portions of this research were carried out on the SXR Instrument at LCLS, a division of SLAC National Accelerator Laboratory and an Office of Science user facility operated by Stanford University for the DOE. The SXR Instrument is funded by a consortium whose membership includes the LCLS, Stanford University through SIMES, Lawrence Berkeley National Laboratory, University of Hamburg through the BMBF priority program FSP 301, and the Center for Free Electron Laser Science.

Supplementary Materials

www.sciencemag.org/cgi/content/full/339/6125/1302/DC1
Materials and Methods
Figs. S1 to S12
References (*28*–*50*)

18 October 2012; accepted 27 December 2012
10.1126/science.1231711

Evidence for Microbial Carbon and Sulfur Cycling in Deeply Buried Ridge Flank Basalt

Mark A. Lever,[1,2]* Olivier Rouxel,[3,4] Jeffrey C. Alt,[5] Nobumichi Shimizu,[3] Shuhei Ono,[6] Rosalind M. Coggon,[7] Wayne C. Shanks III,[8] Laura Lapham,[2]† Marcus Elvert,[9] Xavier Prieto-Mollar,[9] Kai-Uwe Hinrichs,[9] Fumio Inagaki,[10] Andreas Teske[1]*

Sediment-covered basalt on the flanks of mid-ocean ridges constitutes most of Earth's oceanic crust, but the composition and metabolic function of its microbial ecosystem are largely unknown. By drilling into 3.5-million-year-old subseafloor basalt, we demonstrated the presence of methane- and sulfur-cycling microbes on the eastern flank of the Juan de Fuca Ridge. Depth horizons with functional genes indicative of methane-cycling and sulfate-reducing microorganisms are enriched in solid-phase sulfur and total organic carbon, host $\delta^{13}C$- and $\delta^{34}S$-isotopic values with a biological imprint, and show clear signs of microbial activity when incubated in the laboratory. Downcore changes in carbon and sulfur cycling show discrete geochemical intervals with chemoautotrophic $\delta^{13}C$ signatures locally attenuated by heterotrophic metabolism.

Subseafloor basaltic crust represents the largest habitable zone by volume on Earth (*1*). Chemical reactions of basalt with seawater flowing through fractures release energy that may support chemosynthetic communities. Microbes exploiting these reactions are known

Real-Time Observation of Surface Bond Breaking with an X-ray Laser

M. Dell'Angela, T. Anniyev, M. Beye, R. Coffee, A. Föhlisch, J. Gladh, T. Katayama, S. Kaya, O. Krupin, J. LaRue, A. Møgelhøj, D. Nordlund, J. K. Nørskov, H. Öberg, H. Ogasawara, H. Öström, L. G. M. Pettersson, W. F. Schlotter, J. A. Sellberg, F. Sorgenfrei, J. J. Turner, M. Wolf, W. Wurth and A. Nilsson

Science **339** (6125), 1302-1305.
DOI: 10.1126/science.1231711

Surface Molecules Not Quite Desorbing

The dynamics of molecules desorbing from or adsorbing on surfaces requires that molecules rapidly gain or lose a large amount or translational and rotational energy to enter or leave the gas phase. An intermediate precursor state has long been invoked in which molecules interact weakly with the surface but translate along it and exchange energy without forming localized surface bonds. **Dell'Angela *et al.*** (p. 1302) found evidence for such a state in changes in x-ray absorption and emission spectra of CO molecules adsorbed on a ruthenium surface after optical excitation rapidly heated the surface. The use of a free electron laser provided high time resolution for x-ray spectroscopy studies. Density function theory and modeling of high temperature states revealed a state that forms from molecules that have not overcome the desorption barrier during heating and that are bonded less strongly than the chemisorbed state.